RESEARCH PAPER

Multiscale Reconstruction of Near-Wellbore Thermal Memory and Early Multirate Drill Stem Test Inflow after Drilling Circulation

Agus Setiawan,[1] Hendra Wijaya,[2] and Arif Hidayat[3]

[1]Universitas Jenderal Soedirman, Department of Informatics Engineering, HR Boenyamin Street No. 708, Grendeng, Purwokerto 53122, Indonesia
[2]Universitas Negeri Malang, Department of Computer Science, Semarang Street No. 5, Lowokwaru, Malang 65145, Indonesia
[3]Universitas Ahmad Dahlan, Department of Information Systems, Kapas Street No. 9, Umbulharjo, Yogyakarta 55166, Indonesia

Abstract

Thermal disequilibrium around a wellbore can persist for a substantial time after drilling circulation ends, especially in deep or high-temperature settings where the contrast between circulating fluid and native formation temperature is pronounced. This persistence is operationally important because perforation, cleanup, and drill stem testing are often performed before the disturbed rock has fully recovered. Under those circumstances, the earliest fluids entering the wellbore do not represent the undisturbed reservoir alone. Instead, they carry the thermal signature of a near-wellbore region whose temperature has been altered by prior circulation and whose recovery remains incomplete. The result is that early pressure and temperature measurements reflect a coupled transient involving radial heat recovery, inflow redistribution, and wellbore transport rather than a stabilized reservoir response. This paper develops a multiscale reconstruction framework for that problem. The proposed model describes circulation-induced thermal memory in the formation through a reduced radial field, links that field to interval-scale entering fluid temperature by means of an inflow-weighted thermal functional, and embeds the resulting entry conditions into a multirate drill stem test response model. A regularized inverse procedure is then introduced to estimate the hidden thermal state, interval contributions, and uncertain transport parameters from pressure, temperature, and rate data. The analysis emphasizes early-time and late-time asymptotics, identifiability of the disturbed radial profile, and the practical conditions under which thermal memory materially alters inflow interpretation. The resulting formulation is intended to improve early drill stem test diagnostics in recently circulated wells where conventional equilibrium assumptions are not yet valid.

1. Introduction

Interpretation of drill stem test behavior immediately after drilling is often more difficult than the standard pressure-transient formulation suggests (1). The reason is not only that the flow is early or that the well may still be cleaning up. The reason is that the physical state of the formation in the immediate vicinity of the wellbore may still carry a substantial thermal memory of the circulation period that preceded the test. Drilling fluid circulation imposes a thermal forcing on the wellbore and the surrounding rock whenever the fluid temperature differs from the native formation temperature. In high-temperature wells that forcing commonly cools the near-wellbore region, although the same mathematical structure applies to heating in colder settings. Once circulation ceases, that disturbed region does not disappear. It relaxes by radial heat transfer over a timescale controlled by thermal diffusivity, geometric extent of the disturbance, wellbore thermal conductance, and the operational sequence that follows. If perforation, cleanup, and drawdown begin before that relaxation is complete, then the earliest fluid entering the wellbore passes through a radial thermal field that differs from the undisturbed reservoir. Any attempt to infer fluid properties, rate, or effective deliverability from early pressure and temperature data must therefore confront an inherited thermal state that is hidden, spatially distributed, and time dependent.

The near-wellbore cooling problem has direct implications for practical test interpretation because temperature affects several quantities simultaneously (2). Fluid density, viscosity, compressibility, and enthalpy are all temperature dependent. Gas-rich systems are especially sensitive because density and compressibility may shift materially even over modest temperature differences, and volatile or condensate-prone fluids may show further complexity if thermal and pressure transients interact. The thermal state can also influence the effective transmissibility of the very near-wellbore region through temperature-sensitive stress changes, though a purely thermal-flow treatment already reveals much of the interpretive difficulty. What matters for the present paper is that the fluid entering the wellbore during the earliest stages of a drill stem test is not sourced from a thermally neutral formation volume. It is sourced from a region still recovering from circulation. This fact means that early-time wellbore temperature and rate behavior cannot be interpreted correctly through equilibrium assumptions alone.

The operational sequence strengthens the effect. A typical well may experience circulation, cessation of circulation, a period of shut-in, perforation, a cleanup flow, one or more drawdown periods, and one or more buildups, all before the near-wellbore thermal field has stabilized. Each step changes the way measurements relate to the hidden radial temperature state. During circulation, the dominant mechanism is heat exchange between moving wellbore fluid and formation (3). During shut-in, the state evolves mainly by radial heat diffusion

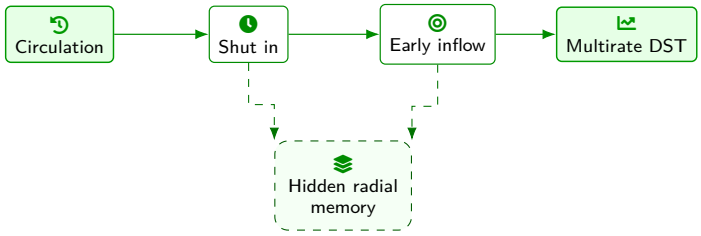


Figure 1. Post-circulation operating window. The sequence emphasizes that early inflow and multirate drill stem testing begin while a latent radial thermal disturbance still persists in the near-wellbore rock, so the test starts from a history-dependent thermal state rather than from equilibrium.

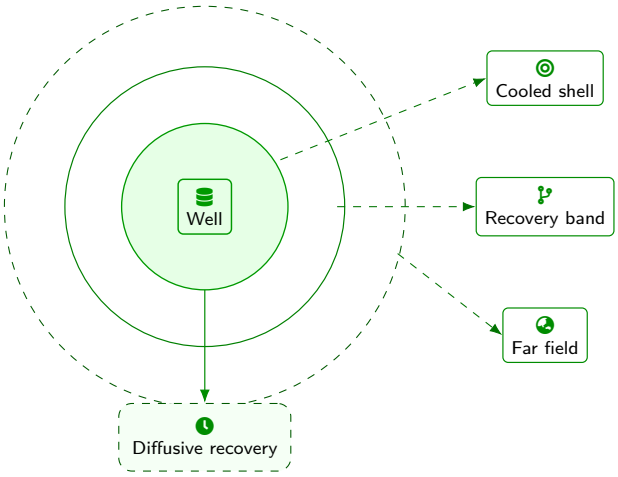


Figure 2. Radial structure of post-circulation thermal memory. The central well is surrounded by a cooled shell and a broader recovery band whose temperature relaxes outward toward the far field by radial diffusion, preserving a distributed thermal memory over the early testing interval.

and residual wellbore equilibration. During early inflow, the temperature of the entering fluid depends on a radial weighting of the disturbed field that is itself controlled by drawdown and local mobility. During multirate flow, rate changes alter that weighting again, so the same hidden radial field is sampled differently from one segment to the next. Because pressure often responds more quickly than temperature, pressure behavior may appear to settle while the thermal field remains strongly transient. A model calibrated mainly to pressure may then misattribute thermal memory to other effects such as effective skin, changing mobility, or measurement irregularity.

A closely related physical motivation appears in the work of Hasan et al. (2024) (4), where circulation-induced near-wellbore cooling is shown to influence the temperature of fluids entering the wellbore and thereby to affect early drill stem test interpretation. The present paper develops a different methodological response in the same field. Rather than centering the analysis on one forward thermal estimate for a given operational schedule, it formulates the problem as a multiscale inverse reconstruction of hidden thermal memory from subsequent test data. In that formulation the disturbed radial temperature field is a latent state (5). Entering fluid temperature is a functional of that latent state. Bottom-hole pressure and temperature are observations generated after the entering fluid mixes, exchanges heat with the wellbore, and evolves under the test schedule. The task of interpretation is then to reconstruct the latent thermal state and its influence on early inflow in a way consistent with both thermal physics and observed well response.

The central thesis of this paper is that early multirate drill stem test interpretation after recent circulation should be posed as a history-dependent thermohydraulic reconstruction problem rather than as a single-regime flow problem with a small temperature correction attached. This thesis has several concrete consequences. First, the thermal disturbance created during circulation must be represented radially rather than collapsed into a scalar offset, because early inflow samples the near-wellbore field nonuniformly and later inflow progressively samples farther radii. Second, the entering fluid temperature should be modeled as an inflow-weighted integral over the disturbed radial field rather than as a boundary temperature at one point. Third, the multirate test schedule is not merely a nuisance. Because rate changes alter the radial weighting of the hidden thermal field, they provide information about that field when interpreted appropriately. Fourth, inversion must be regularized by the physical structure of heat diffusion, because the hidden state is only partially observable and several thermal and hydraulic parameters can compensate one another over short windows (6).

The strategy adopted here is therefore to build an analytic and reduced-order structure around the thermal memory of circulation. The first part of the paper formalizes the physical

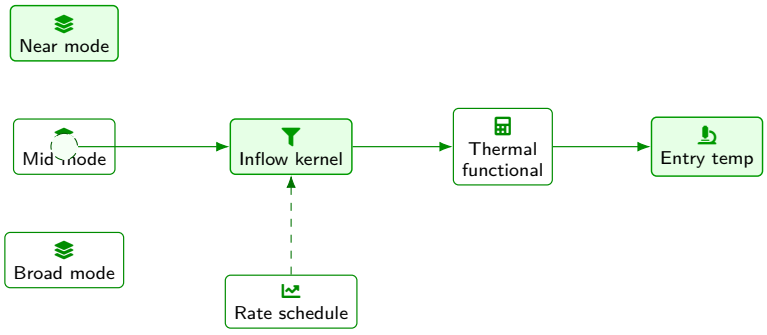


Figure 3. Reduced reconstruction of entering-fluid temperature. The hidden radial field is represented by a small set of thermal modes, the rate-dependent inflow kernel determines how those modes are sampled, and the resulting functional produces the interval entry temperature that carries the near-wellbore thermal memory into the test response.

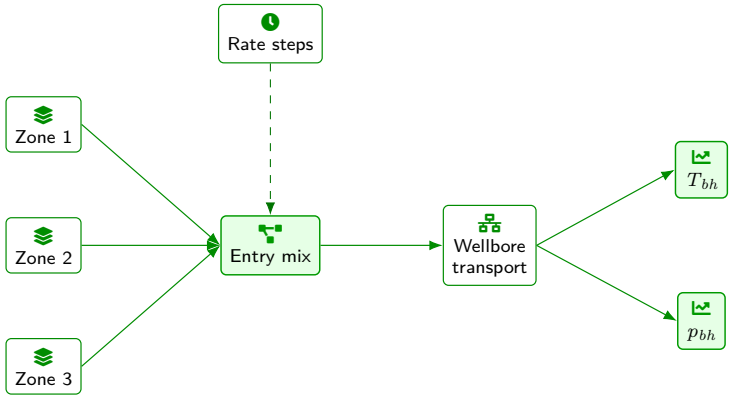


Figure 4. Multirate drill stem test response with distributed inflow and wellbore transport. Interval-specific entry streams are mixed, advected, and thermally exchanged in the wellbore before the bottom-hole temperature and pressure are observed, while rate steps modify both inflow partitioning and thermal sampling.

setting and identifies the relevant timescales. The next part derives an integral representation of radial thermal memory and shows how it enters the entering-fluid temperature. The analysis then couples this entry-temperature model to a multirate drill stem test response equation that includes distributed inflow, wellbore thermal transport, and compressible effects in reduced form. On that basis a regularized inverse reconstruction is developed. The inverse formulation estimates the hidden radial thermal coefficients, interval-scale contribution factors, and uncertain thermal transport parameters from measured pressure, temperature, and rate histories. An asymptotic section follows, because early-time and late-time limits illuminate which parts of the hidden field are actually observable from field data. The paper then turns to numerical design and field-oriented interpretation logic, emphasizing what kinds of tests can truly constrain the thermal memory and which ambiguities remain irreducible.

The intention is not to claim that a single reduced inverse framework resolves every complexity of well testing after circulation. Wells may be multilayered, multiphase, deviated, or compositionally complicated (7). Those issues can all matter. The narrower but important claim made here is that delayed near-wellbore thermal recovery is a first-order interpretive variable in recently circulated wells and that it can be represented mathematically in a way that is both physically transparent and operationally useful. By organizing the problem around hidden radial thermal memory rather than around isolated temperature corrections, one can obtain a more coherent picture of early inflow temperature, interval contribution, and multirate test behavior.

2. Physical Setting and Time-Scale Structure of Post-Circulation Thermal Memory

The essential physical object in the present problem is the temperature disturbance in the formation immediately surrounding the wellbore. Let r denote radial distance from the well axis, r_w the effective wellbore or completion radius, and r_b an outer radius large enough that the temperature disturbance is negligible there on the timescale of interest. Let the undisturbed formation temperature at the tested interval be T_∞, and define the disturbed field as

$$\theta r, t = T_f r, t - T_\infty. \tag{2.1}$$

When circulation fluid is cooler than the formation, $\theta r, t$ is negative near the wellbore after circulation ends. The quantity of direct operational interest is not θ at one point but the way the entire radial profile evolves and how it influences the temperature of fluid entering the wellbore during the test.

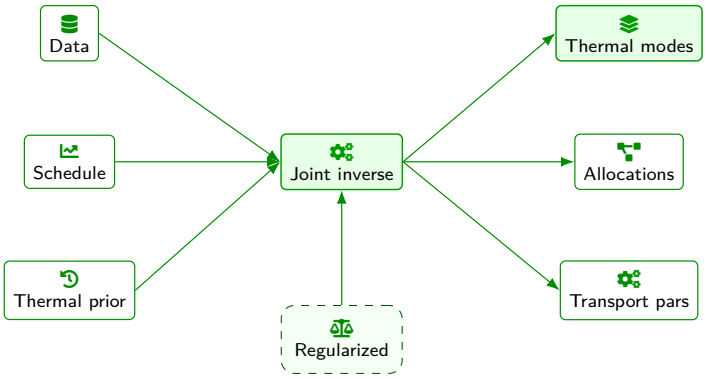


Figure 5. Regularized inverse reconstruction. Pressure, temperature, and rate history are fused with operational schedule and circulation-informed priors to recover latent thermal modes, interval contribution factors, and uncertain transport parameters under a physically constrained joint inversion.

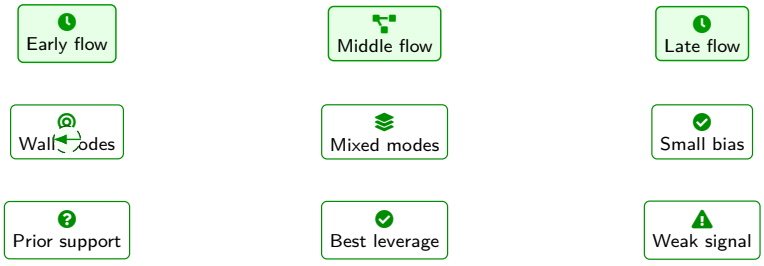


Figure 6. Asymptotic observability structure. Early flow mainly resolves the near-wall thermal modes, intermediate multirate response offers the strongest leverage on a broader subset of hidden states, and late recovery carries a weaker but more equilibrated thermal signal as the circulation imprint decays.

The thermal evolution of the formation in a single tested interval may be represented by an effective radial energy equation. Neglecting azimuthal variation and suppressing depth dependence locally, one has (8)

$$\rho c_e \frac{\partial T_f}{\partial t} \; \rho c_m v_r \frac{\partial T_f}{\partial r} = \frac{1}{r}\frac{\partial}{\partial r}\left(k_e r \frac{\partial T_f}{\partial r}\right) \; q_h r, t, \tag{2.2}$$

where ρc_e is the effective volumetric heat capacity of the saturated formation, ρc_m is the mobile fluid contribution, v_r is radial Darcy velocity during inflow, k_e is effective thermal conductivity, and q_h is a source term representing reduced interaction with the wellbore or other unresolved mechanisms. In terms of the disturbance θ, and assuming the far-field temperature is stationary over the relevant operational window, the same equation becomes

$$\rho c_e \frac{\partial \theta}{\partial t} \; \rho c_m v_r \frac{\partial \theta}{\partial r} = \frac{1}{r}\frac{\partial}{\partial r}\left(k_e r \frac{\partial \theta}{\partial r}\right) \; q_h r, t. \tag{2.3}$$

During shut-in before flow begins, the radial velocity is negligible and the equation is essentially diffusive. During flow, the advective term becomes important near the wellbore where the inflowing fluid is sampling the recovering thermal field.

A useful first observation concerns timescale separation. The characteristic radial thermal recovery time over a radial scale L_r is approximately

$$\tau_T \sim \frac{L_r^2}{\alpha}, \tag{2.4}$$

where $\alpha = k_e \rho c_e$ is thermal diffusivity. By contrast, a characteristic hydraulic response time over the same interval depends on pressure diffusivity and well conditions and may be considerably shorter. This difference matters because pressure data can give the appearance of stabilization while the thermal field remains strongly transient. If the near-wellbore thermal disturbance extends several inches or more into a low-diffusivity formation, the recovery time may exceed the earliest drawdown and cleanup periods by a substantial margin (9). In that case, any early-time entering temperature must be interpreted as a transient sampling of a recovering radial field rather than as a reservoir temperature proxy.

The wellbore itself introduces another timescale. Let $T_w z, t$ denote wellbore fluid temperature in the tested interval. Its evolution may be represented through a reduced axial energy balance,

$$\frac{\partial}{\partial t}\left(\rho_w A_w c_{p,w} T_w\right) \; \frac{\partial}{\partial z}\left(m h_w\right) = U P \left(T_f r_w, z, t - T_w\right) \; Q_m z, t, \tag{2.5}$$

where ρ_w is wellbore fluid density, A_w the flow area, $c_{p,w}$ the specific heat, m the mass flow rate, h_w the enthalpy, U an overall heat-transfer coefficient, P wetted perimeter, and Q_m a reduced source term accounting for inflow mixing and additional thermal effects. The wellbore thermal response is influenced by entering fluid enthalpy and by continued exchange with the disturbed formation. Thus the measured bottom-hole temperature does not reveal the entering temperature directly. It is the

Table 1. Primary symbols used in the thermohydraulic formulation

Symbol	Description	Units	Section Context
r	Radial distance from well axis	m	Thermal field definition
r_w	Effective wellbore radius	m	Near-wellbore boundary
T_∞	Undisturbed formation temperature	K	Far-field reference
$\theta r, t$	Thermal disturbance $T_f - T_\infty$	K	Radial memory state
k_e	Effective thermal conductivity	W m^{-1}K^{-1}	Formation heat transfer
α	Thermal diffusivity $k_e \rho c_e$	m^{2}s^{-1}	Recovery timescale

Table 2. Characteristic time scales governing post-circulation thermal recovery

Process	Characteristic Expression	Physical Meaning	Operational Impact
Radial thermal recovery	$\tau_T \sim L_r^2 \alpha$	Diffusive relaxation of disturbance	Controls persistence of cooling
Hydraulic pressure response	τ_P (pressure diffusivity)	Pressure propagation in formation	Faster than thermal response
Wellbore equilibration	τ_W	Thermal exchange with formation	Alters measured temperature
Operational sequence	τ_O	Shut-in and flow scheduling	Determines sampling of thermal state

result of a transient coupling among inflow, wellbore transport, and the surrounding rock.

The radial disturbance at the end of circulation is determined by the circulation history. If $q_c\tau$ denotes an effective thermal forcing at the wellbore during circulation, a line-source style representation yields a history-dependent radial field for later times,

$$\theta r, t = -\int_0^{t_c} \frac{q_c \tau}{4\pi k_e H} E_1\left(\frac{r^2}{4\alpha t - \tau}\right) d\tau, \quad t > t_c, \tag{2.6}$$

where t_c is the end of circulation, H is an effective interval thickness, and E_1 is the exponential integral (10). This expression is not intended as an exact universal solution for every completion geometry. Its importance lies in showing that circulation does not produce a single thermal offset. It produces a distributed radial memory kernel that decays diffusively and whose shape depends on the time history of thermal forcing.

The operational sequence after circulation determines how that hidden memory becomes observable. During pure shut-in, observations of temperature at the wellbore mainly reveal how the wall-adjacent portion of the field is recovering and how the wellbore column itself is equilibrating. During initial flow, the relevant quantity becomes the temperature of the fluid as it enters the well. This temperature depends on a radial weighting of the disturbed field. Early in the flow period the weighting is heavily concentrated near the wellbore because the pressure perturbation has not penetrated far. Later, the weighting broadens. A multirate schedule changes the weighting again (11). Thus the test itself probes the hidden radial field with a sequence of different filters. That fact is central to the reconstruction approach developed later in the paper.

Another important aspect is multilayer or multi-entry behavior. If several perforated intervals contribute flow, each may possess a different thermal history. One interval may have experienced stronger cooling because of local circulation exposure or longer contact with a cooler fluid column. Another may have recovered more during shut-in because of higher diffusivity or thinner damaged zone. These differences can lead to interval-specific entering temperatures even when the far-field geothermal temperature does not vary strongly. When those streams mix in the wellbore, the measured temperature becomes a weighted mixture of hidden interval contributions. The inverse problem is therefore not only radial but also compositional across entries.

The physical setting is therefore governed by three interlocking facts (12). First, near-wellbore thermal memory is radially distributed and persists after circulation. Second, the test schedule probes that memory through time-varying inflow and wellbore transport. Third, the measured temperature is a mixed response rather than a direct state variable. These facts motivate a formulation in which circulation history enters through a thermal memory kernel, inflow is treated as a weighted sampling of that kernel, and interpretation proceeds by reconstructing the hidden radial state from the available data. The next section formalizes the thermal memory kernel and derives the integral relation connecting it to entering fluid temperature.

3. Thermal Memory Kernel and the Reconstruction of Entering Fluid Temperature

The central hidden quantity for early drill stem test interpretation is the radial thermal profile in the near-wellbore zone. Yet the immediate practical quantity of interest is not the full profile itself. It is the temperature of the fluid entering the wellbore after passing through that disturbed zone. Bridging those two quantities requires a mathematically explicit thermal memory kernel and a carefully defined inflow weighting.

A useful reduced description begins by separating the radial disturbance from the far field and expanding the disturbance in a finite basis, (13)

$$\theta r, t = \sum_{i=1}^{M} a_i t \phi_i r, \tag{3.1}$$

where $\{\phi_i r\}$ are radial basis functions chosen to resolve the thermally important scales of the near-wellbore region. The basis may be constructed from diffusion eigenfunctions, logarith-

Table 3. Components of the radial thermal memory representation

Component	Mathematical Form	Interpretation	Role in Model
Basis functions	$\phi_i r$	Radial temperature modes	Resolve near-wellbore gradients
Coefficients	$a_i t$	Time-dependent amplitudes	Hidden thermal memory state
Mode expansion	$\theta r, t = a_i t \phi_i r$	Reduced representation	Enables inversion
Recovery propagator	G_k	Diffusive temporal evolution	Controls mode decay

Table 4. Key quantities describing entering fluid temperature

Quantity	Definition	Dependence	Physical Meaning
$T_{\mathrm{in}} t$	Entering fluid temperature	Radial disturbance	Inflow thermal state
$w r, t$	Inflow weighting kernel	Flow dynamics	Radial sampling function
$c_i t$	Mode observation weight	Kernel and basis	Projection of thermal modes
ΔT_{bias}	$T_\infty - T_{\mathrm{in}}$	Thermal memory	Property bias indicator

mic finite-volume hat functions, or orthonormalized circulation-recovery snapshots. What matters is that the first few modes capture the steep gradients close to r_w, because early inflow is most sensitive to those gradients. The coefficients $a_i t$ form the latent thermal memory state. During shut-in, their evolution is predominantly diffusive. During flow, advection and changing boundary conditions perturb their dynamics, but the same coefficients still retain a consistent physical meaning.

The entering temperature $T_{\mathrm{in}} t$ is modeled as a radial functional of $\theta r, t$. Let $w r, t$ denote the inflow weighting kernel, which represents the contribution of each radial shell to the fluid entering the well at time t. Then

$$T_{\mathrm{in}} t = T_\infty \frac{\int_{r_w}^{r_b} w r, t \theta r, t \, dr}{\int_{r_w}^{r_b} w r, t \, dr}. \tag{3.2}$$

This formula encodes a simple but important physical fact: the inflowing fluid does not sample the near-wellbore region uniformly. The weighting is concentrated near the wellbore at early time, then broadens as the pressure transient penetrates farther outward. The exact kernel depends on compressibility, mobility, skin, and completion details, but its qualitative structure is robust.

Substituting the basis expansion into the entering-temperature formula gives (14)

$$T_{\mathrm{in}} t = T_\infty \sum_{i=1}^{M} c_i t a_i t, \tag{3.3}$$

where

$$c_i t = \frac{\int_{r_w}^{r_b} w r, t \phi_i r \, dr}{\int_{r_w}^{r_b} w r, t \, dr}. \tag{3.4}$$

The coefficients $c_i t$ are the effective thermal observation weights induced by the inflow at time t. This representation makes the interpretation problem clearer. The hidden thermal memory state is the vector $a t$. The entering temperature is a time-varying linear functional of that state. When the rate changes, the kernel $w r, t$ changes, and hence the vector $c t$ changes. Thus the multirate test naturally provides several different projections of the same hidden radial field.

The inflow kernel can be related to pressure-transient structure. In a single-phase radial inflow setting, one may take

$$w r, t \propto r \rho r, t |v_r r, t|, \tag{3.5}$$

so that radial shells contribute in proportion to mass flux. Alternative choices are possible, especially when the aim is to approximate the residence-time distribution of fluid particles moving toward the well (15). The present formulation leaves the exact kernel general because the crucial point is its operational dependence, not a single fixed closed-form expression. In a reduced inverse model, $w r, t$ may be precomputed over a range of representative flow conditions or expressed through a parameterized family indexed by drawdown and mobility.

During the earliest portion of a flow period, the kernel is sharply concentrated near the wellbore. If the basis functions are ordered from near-wall to broader scales, then the entering temperature admits an early-time approximation

$$T_{\mathrm{in}} t = T_\infty \sum_{i=1}^{m_e} c_i^e t a_i t \, \mathcal{O} \epsilon_t, \tag{3.6}$$

where $m_e \ll M$ and ϵ_t measures the small contribution of broader modes at very early time. This approximation implies that early-time temperature data strongly identify only a narrow projection of the thermal memory state. It also explains why scalar correction formulas often fail: they effectively assume $m_e = 1$ and neglect the broader basis of radial disturbance needed as the test evolves.

The same logic applies to multilayer inflow. Suppose interval ℓ has its own thermal memory state $a^\ell t$ and weighting vector $c^\ell t$. Then its entering temperature is

$$T_{\mathrm{in}}^\ell t = T_\infty^\ell \, c^\ell t^\top a^\ell t. \tag{3.7}$$

If $m_\ell t$ is the interval mass inflow, the mixed entry temperature at the wellbore is related to the interval contributions through enthalpy conservation. In the simplest single-phase approximation, (16)

$$T_{\mathrm{mix}} t \approx \frac{\sum_{\ell=1}^{L} m_\ell t c_{p,\ell} t T_{\mathrm{in}}^\ell t}{\sum_{\ell=1}^{L} m_\ell t c_{p,\ell} t}, \tag{3.8}$$

Table 5. Interval-scale variables in distributed inflow modeling

Variable	Description	Model Role	Observational Link
$m_\ell t$	Mass inflow from interval ℓ	Distributed inflow	Affects pressure and temperature
T_{in}^{ℓ}	Interval entering temperature	Thermal state per layer	Enthalpy source
$\zeta_\ell t$	Soft allocation variable	Flow distribution control	Determines interval contribution
$p_{r,\ell}$	Effective reservoir pressure	Inflow driving force	Appears in inflow law

Table 6. Elements of the reduced wellbore thermal transport model

Element	Mathematical Quantity	Function	Measurement Influence
Wellbore temperature	$T_w z, t$	Axial thermal state	Produces measured temperature
Mass flow	mz, t	Energy transport	Couples entries along wellbore
Heat transfer coefficient	U	Formation–wellbore exchange	Controls thermal relaxation
Entry enthalpy	h_ℓ^{in}	Interval thermal input	Drives mixing temperature

where $c_{p,\ell} t$ are effective heat capacities. Even if the completion intervals are similar hydraulically, distinct thermal histories can therefore produce different interval entering temperatures and hence a mixed temperature response that cannot be captured by a single-layer model.

The thermal memory kernel also clarifies the role of shut-in duration. Let t_s denote the shut-in start and t_f the start of flow. The radial state at the start of flow is

$$a t_f^- = \mathcal{G} t_f - t_s a t_s \int_{t_s}^{t_f} \mathcal{G} t_f - \tau f_w \tau \, d\tau, \tag{3.9}$$

where $\mathcal{G}$ is the reduced recovery propagator and f_w is the effective wall forcing induced by residual wellbore equilibration. Thus shut-in time enters the problem through a semigroup action on the post-circulation thermal state. Two wells with identical circulation histories but different shut-in durations can therefore have markedly different entering temperatures at the start of testing, even if their pressure conditions are comparable.

Another instructive quantity is the thermal bias relative to the undisturbed formation temperature,

$$\Delta T_{\text{bias}} t = T_\infty - T_{\text{in}} t. \tag{3.10}$$

This bias can be propagated directly into fluid-property corrections. If μT and ρT are local viscosity and density relations, then to first order

$$\begin{aligned} \Delta \mu t &\approx \frac{\partial \mu}{\partial T}\Big|_{T=T_\infty} \Delta T_{\text{bias}} t \\ \Delta \rho t &\approx \frac{\partial \rho}{\partial T}\Big|_{T=T_\infty} \Delta T_{\text{bias}} t. \end{aligned} \tag{3.11}$$

In gas systems this bias can influence rate estimates and apparent deliverability (17). That is why accurate reconstruction of $T_{\text{in}} t$ matters even when the primary operational quantity of interest is not temperature itself.

The thermal memory kernel therefore provides both a conceptual and mathematical bridge between circulation history and early drill stem test inflow. It converts the hidden radial profile into a time-varying, schedule-dependent inflow temperature. Once combined with a wellbore transport model, it produces the measured temperature response. The next section incorporates this structure into a multirate drill stem test model suitable for inversion.

4. Multirate Drill Stem Test Response with Distributed Inflow and Wellbore Thermal Transport

A thermal reconstruction is only useful if it can be linked directly to the observables measured during the test. In practice those observables include bottom-hole pressure, bottom-hole temperature, and one or more measures of rate or choke condition. The physical relation between the hidden radial thermal memory and those observables is mediated by distributed inflow and by the thermal transport of the wellbore fluid.

Let z denote depth along the relevant wellbore segment and $T_w z, t$ the flowing fluid temperature. Let inflow occur at L entry locations z_ℓ, each with mass rate $m_\ell t$ and interval-specific entering enthalpy $h_\ell^{\text{in}} t$. The reduced energy balance for the flowing wellbore is

$$\begin{aligned} \frac{\partial}{\partial z}\left(mz, t h_w z, t\right) = {} & Uz, tPz\left(T_f r_w, z, t - T_w z, t\right) \\ & \sum_{\ell=1}^{L} m_\ell t h_\ell^{\text{in}} t \delta z - z_\ell \;\; Q_\ell z, t, \end{aligned} \tag{4.1}$$

where Q_ℓ is a reduced source term representing axial effects not explicitly resolved elsewhere (18). The enthalpy of the entering stream is determined from the interval entering temperature, pressure, and fluid properties:

$$h_\ell^{\text{in}} t = h\left(T_{\text{in}}^{\ell} t, p_\ell t\right). \tag{4.2}$$

Thus the hidden thermal memory state influences the measured wellbore temperature through the interval enthalpy sources.

The pressure model is coupled but need not be resolved at the same level of detail as a full reservoir simulator for the purposes of interpretation. A reduced inflow law is sufficient if it preserves the sensitivity of interval rate to bottom-hole pressure and local conditions. For each interval ℓ,

$$m_\ell t = \mathcal{Q}_\ell \left(p_{r,\ell}, p_{bh} t, \mu_\ell T_{\text{in}}^{\ell}, \rho_\ell T_{\text{in}}^{\ell}, \kappa_\ell t\right), \tag{4.3}$$

Table 7. State-space structure used in the reconstruction framework

State Component	Symbol	Description	Dynamics Source
Thermal coefficients	a_k^ℓ	Radial disturbance modes	Diffusion recovery
Wellbore thermal state	b_k	Reduced wellbore energy state	Axial transport
Allocation variables	ζ_k	Interval contribution weights	Inflow redistribution
Parameter vector	ϑ_k	Diffusivity, conductance, etc.	Transport properties

Table 8. Regularization terms used in inverse reconstruction

Regularizer	Mathematical Form	Purpose	Physical Motivation
Thermal evolution	$\mathcal{R}_{th}a$	Stabilize thermal modes	Diffusive recovery constraint
Allocation smoothness	$\mathcal{R}_{alloc}\zeta$	Prevent abrupt flow shifts	Physical interval continuity
Parameter prior	$\mathcal{R}_\vartheta\vartheta$	Enforce admissible values	Transport realism
Initial state prior	$a_0 \sim m_0$	Circulation-based estimate	Encodes thermal history

where $p_{r,\ell}$ is an effective reservoir pressure, $p_{bh}t$ the bottom-hole pressure, and $\kappa_\ell t$ a reduced interval factor accounting for skin, completion loss, or changing effective transmissibility. The dependence of m_ℓ on T_{in}^ℓ arises through viscosity, density, and possibly compressibility. Thus the thermal memory state can affect rate not only through the temperature measurement but also through the inflow law itself.

A convenient reduced parameterization of interval contribution uses soft allocation variables $\zeta_\ell t$,

$$m_\ell t = m_{\text{tot}}t\frac{\exp\zeta_\ell t}{\sum_{j=1}^{L}\exp\zeta_j t}. \tag{4.4}$$

This parameterization is useful even when total rate is observed because it separates overall drawdown from interval distribution. The $\zeta_\ell t$ variables are then estimated jointly with the thermal coefficients (19). If one interval remains more strongly cooled than another, its contribution to the mixed wellbore temperature can be thermally identifiable even when pressure alone provides only weak discrimination.

The multirate schedule affects the model through both $m_{\text{tot}}t$ and the interval weighting vectors $c^\ell t$. Consider a rate change at time t_r. Immediately before the change the entering temperatures are

$$T_{\text{in}}^\ell t_r^- = T_\infty^\ell \;\; c_-^{\ell\top} a^\ell t_r^-. \tag{4.5}$$

Immediately after the rate change, the thermal coefficients $a^\ell t_r$ remain continuous to leading order because the radial field does not jump. However the weighting vectors shift,

$$T_{\text{in}}^\ell t_r = T_\infty^\ell \;\; c^{\ell\top} a^\ell t_r. \tag{4.6}$$

The difference between c_-^ℓ and c^ℓ can create an observable thermal effect even when the underlying radial field changes only slowly across the same instant. This fact is valuable because it means multirate schedules provide more than extra pressure transients. They also provide multiple thermal views of the same hidden radial state.

The measured bottom-hole temperature is then obtained after wellbore mixing and transport. In a reduced model one may express it as

$$T_{bh}t = \mathcal{W}\left(\{T_{\text{in}}^\ell t\}_{\ell=1}^L, \{m_\ell t\}_{\ell=1}^L, bt, ut\right), \tag{4.7}$$

where bt denotes the reduced wellbore thermal state and ut operational inputs. Similarly the measured bottom-hole pressure satisfies (20)

$$p_{bh}t = \mathcal{P}\left(\{m_\ell t\}_{\ell=1}^L, qt, ut\right). \tag{4.8}$$

The two observations are therefore coupled through the same hidden interval flows and through the thermal state. This is why a joint inversion is more informative than a separate treatment of temperature and pressure.

The system can now be written as a reduced nonlinear state-space model. Let

$$x_k = \begin{bmatrix} a_k^1 \\ \vdots \\ a_k^L \\ b_k \\ \zeta_k \\ \vartheta_k \end{bmatrix}. \tag{4.9}$$

Then the discrete transition over one observation interval is

$$x_{k1} = A_{\sigma_k}x_k \;\; B_{\sigma_k}u_k \;\; r_{\sigma_k}x_k, u_k \;\; \epsilon_k, \tag{4.10}$$

and the observation map is

$$y_k = \begin{bmatrix} T_{bh,k} \\ p_{bh,k} \\ m_{\text{tot},k} \end{bmatrix} = \mathcal{H}_{\sigma_k}x_k, u_k \;\; \eta_k. \tag{4.11}$$

The operational mode σ_k encodes shut-in, drawdown at a particular rate, buildup, and other scheduled segments. The hidden thermal memory state persists across those modes even as the observation operator changes. It is precisely this mode-dependent but state-continuous structure that the inverse reconstruction must respect.

Table 9. Performance metrics used in numerical validation

Metric	Expression	Evaluated Quantity	Interpretation
Entering temperature error	$\mathcal{E}_{T_{in}}$	Reconstructed inflow temperature	Thermal accuracy
Interval temperature error	$\mathcal{E}^{\ell}_{T_{in}}$	Layer-specific inflow temperature	Interval resolution
Rate reconstruction error	$\mathcal{E}_q$	Predicted flow rate	Hydraulic accuracy
Transition adaptation loss	$\mathcal{A}k^{\star}, H$	Response after rate change	Multirate adaptability

Table 10. Asymptotic regimes of temperature response during testing

Regime	Dominant Mechanism	Observable Features	Interpretation Impact
Early-time flow	Near-wall thermal modes	Strong temperature deviation	Constrains shallow disturbance
Intermediate time	Broad radial sampling	Multiple thermal modes visible	Improved identifiability
Late-time recovery	Weak residual disturbance	Temperature approaches T_{∞}	Thermal memory fades
Post-recovery	Equilibrium state	Minimal thermal bias	Standard interpretation valid

What this section establishes is that the measurement sequence in a multirate drill stem test is generated by a composition of maps: circulation history shapes the hidden radial thermal memory, the hidden thermal memory shapes the entering temperatures, the entering temperatures and interval flows shape the wellbore thermal state, and the wellbore thermal state together with bottom-hole pressure produces the measured data. The inverse problem must therefore work backward through this chain (21). The next section develops a regularized reconstruction procedure for doing so.

5. Regularized Inverse Reconstruction of Hidden Thermal Memory and Interval Contribution

The reduced multirate thermohydraulic model permits interpretation to be stated as an inverse problem over hidden states and uncertain parameters. Let the unknowns over an observation window be the interval thermal coefficient trajectories a^{ℓ}_k, the wellbore thermal states b_k, the interval contribution variables ζ_k, and a parameter vector ϑ containing effective diffusivities, wall conductances, and selected correction factors. Let y_k be the measured data and u_k the known operational inputs. The goal is to recover the hidden quantities in a way that fits the data while remaining consistent with the dissipative structure of thermal recovery and with physically admissible interval behavior.

A natural formulation is a dynamic regularized least-squares functional. Denote the full hidden state by x_k and the reduced forward maps by $\mathcal{F}_k$ and $\mathcal{H}_k$. The objective is

$$\begin{aligned}\mathcal{J}\, x_{0:N}, \vartheta = \frac{1}{2} \sum_{k=0}^{N} \left(y_k - \mathcal{H}_k x_k, u_k, \vartheta\right)^{\top} R_k^{-1} \left(y_k - \mathcal{H}_k x_k, u_k, \vartheta\right) \\ \frac{1}{2} \sum_{k=0}^{N-1} \left(x_{k1} - \mathcal{F}_k x_k, u_k, \vartheta\right)^{\top} Q_k^{-1} \left(x_{k1} - \mathcal{F}_k x_k, u_k, \vartheta\right) \\ \mathcal{R}_{\mathrm{th}}\, a_{0:N}\ \mathcal{R}_{\mathrm{alloc}} \zeta_{0:N}\ \mathcal{R}_{\vartheta} \vartheta. \end{aligned} \tag{5.1}$$

The first term measures the data mismatch. The second penalizes deviations from the reduced dynamical model. The remaining three terms impose thermal, allocation, and parameter regularization. These regularizers are not generic smoothness penalties (22). They encode specific physics of the near-wellbore problem.

The thermal regularizer should reflect the fact that post-circulation recovery is diffusion dominated and radially smooth in an appropriate basis. A useful form is

$$\mathcal{R}_{\mathrm{th}}\, a_{0:N} = \frac{\lambda_a}{2} \sum_{\ell=1}^{L} \sum_{k=0}^{N-1} \left\| a^{\ell}_{k1} - G^{\ell}_k a^{\ell}_k \right\|_2^2 \frac{\lambda_0}{2} \sum_{\ell=1}^{L} \left\| a^{\ell}_0 - m^{\ell}_0 \right\|^2_{P_0^{\ell-1}}, \tag{5.2}$$

where G^{ℓ}_k is the nominal reduced recovery propagator for interval ℓ and m^{ℓ}_0 is a prior mean derived from circulation history. This term prevents the inversion from fitting the data by introducing thermally implausible oscillation in the hidden radial field.

The interval-allocation regularizer reflects the fact that contribution fractions should not swing erratically unless the data strongly support such change. If ζ_k denotes the vector of soft allocation variables, one may set

$$\mathcal{R}_{\mathrm{alloc}} \zeta_{0:N} = \frac{\lambda_{\zeta}}{2} \sum_{k=0}^{N-1} \|\zeta_{k1} - \zeta_k\|_2^2 \frac{\lambda_s}{2} \sum_{k=0}^{N} \sum_{\ell=1}^{L} \left(\zeta_{\ell,k} - \bar{\zeta}_{\ell,k}\right)^2, \tag{5.3}$$

where $\bar{\zeta}_{\ell,k}$ is a weak prior trajectory based on interval transmissibility expectations. This regularization is important because a temperature mismatch can sometimes be explained either by adjusting the thermal memory state or by changing the allocation. The inversion should not choose between those explanations based on local noise.

The parameter regularizer ensures physical admissibility and protects directions that are poorly identified by short windows. For transformed positive parameters ϑ, (23)

$$\mathcal{R}_{\vartheta} \vartheta = \frac{1}{2} \vartheta - \vartheta_0{}^{\top} W^{-1} \vartheta - \vartheta_0\ \lambda_p \sum_j \Phi_j \vartheta_j, \tag{5.4}$$

where W is a prior covariance and Φ_j penalizes nonphysical values or departures from dissipative structure. For example, diffusivity and conductance must remain positive, and combinations of parameters that would produce amplifying thermal modes can be excluded or heavily penalized.

The gradient of $\mathcal{J}$ with respect to hidden states and parameters is obtained through an adjoint recursion. Let λ_k denote the adjoint variable at time k. Then

$$\lambda_N = \left(\partial_{x_N}\mathcal{H}_N\right)^\top R_N^{-1}\left(y_N - \mathcal{H}_N\right) - \partial_{x_N}\mathcal{R}_{\text{th}} - \partial_{x_N}\mathcal{R}_{\text{alloc}}, \tag{5.5}$$

and for $k = N-1, \ldots, 0$,

$$\lambda_k = \left(\partial_{x_k}\mathcal{F}_k\right)^\top Q_k^{-1}\left(x_{k1} - \mathcal{F}_k\right) \left(\partial_{x_k}\mathcal{H}_k\right)^\top R_k^{-1}\left(y_k - \mathcal{H}_k\right) \left(\partial_{x_k}\mathcal{F}_k\right)^\top \lambda_{k1} - \partial_{x_k}\mathcal{R}_{\text{th}} - \partial_{x_k}\mathcal{R}_{\text{alloc}}. \tag{5.6}$$

The parameter gradient is

$$\nabla_\vartheta \mathcal{J} = -\sum_{k=0}^{N}\left(\partial_\vartheta \mathcal{H}_k\right)^\top R_k^{-1}\left(y_k - \mathcal{H}_k\right) - \sum_{k=0}^{N-1}\left(\partial_\vartheta \mathcal{F}_k\right)^\top Q_k^{-1}\left(x_{k1} - \mathcal{F}_k\right) - \sum_{k=0}^{N-1}\left(\partial_\vartheta \mathcal{F}_k\right)^\top \lambda_{k1} \nabla_\vartheta \mathcal{R}_\vartheta. \tag{5.7}$$

These expressions make it practical to use Gauss-Newton or projected quasi-Newton updates even when the full trajectory is estimated.

Several structural observations follow immediately. The hidden thermal coefficients a_k^ℓ affect the objective directly through measured temperature and indirectly through interval rates and pressure, since T_{in}^ℓ enters the property-dependent inflow law. The allocation variables ζ_k affect the mixed wellbore temperature through interval weighting and affect the measured pressure through distributed inflow. The parameters ϑ affect both the recovery dynamics and the observation map. Because these effects are coupled, fitting temperature alone or pressure alone can produce biased latent-state reconstructions (24). Joint inversion is not a luxury here; it is a structural necessity.

For operational use, the full-horizon inversion may be approximated by a sliding-window reconstruction in which the latest W samples are re-estimated whenever new data arrive. The initial condition of each window is given by the filtered estimate from the previous window, and a few adjoint iterations are sufficient to refine the thermal memory state and interval contributions. This permits quasi-online use without abandoning the full dynamical structure.

The inverse reconstruction is therefore built around one principle: the hidden thermal memory of circulation should be recovered from the test in a way consistent with diffusion, wellbore transport, and interval mixing, rather than through ad hoc correction factors. The next section shows why this approach is especially informative when the early and late asymptotics of the test are analyzed explicitly.

6. Asymptotic Structure, Observability, and Interpretive Limits

One of the most useful ways to understand the reconstruction problem is through its early-time and late-time asymptotics. These limits reveal which parts of the hidden thermal memory state are observable from the data and which remain effectively unconstrained without stronger prior information or different measurements.

At very early flow times after shut-in, the inflow weighting kernel is concentrated close to the wellbore. If the basis functions are ordered from most localized near r_w to most extended, then the entering temperature admits the asymptotic form (25)

$$T_{\text{in}}t = T_\infty \sum_{i=1}^{m_e} c_i^e t a_i t \; \mathcal{O}\left(\varepsilon_t\right), \tag{6.1}$$

where m_e is small and ε_t is the residual contribution of broader radial modes. This expression implies that early-time temperature is sensitive mainly to the shallowest portion of the disturbed zone. Therefore the earliest measured temperature data constrain the near-wall thermal modes strongly but say relatively little about the deeper extent of cooling. If one tries to reconstruct the entire radial profile from a short early-time record, the result is inevitably prior dominated. What the data truly support is a narrow projection of the profile.

This early-time asymptotic picture also explains why different physical mechanisms can be confounded. A stronger near-wall thermal deficit, a larger inflow fraction from a colder interval, or a slightly larger wellbore heat-loss coefficient can all depress the measured bottom-hole temperature over a short time window. Pressure data help separate these explanations because interval fraction and hydraulic properties influence pressure differently from pure thermal recovery. Yet even with joint pressure-temperature data, the earliest window is typically insufficient to resolve all broad thermal modes and all interval allocations uniquely. The correct response is not to force the inversion to one apparent solution, but to regularize the ill-conditioned directions and propagate the associated uncertainty (26).

At intermediate times, the pressure perturbation expands radially and the inflow weighting broadens. More thermal modes begin to contribute to the entering temperature. At the same time, the amplitude of the disturbance decreases as recovery proceeds. Thus information increases in dimension but may decrease in signal strength. This trade-off is one reason multirate schedules can be useful. A rate increase or decrease changes the weighting vector and effectively provides a new projection of the same hidden thermal state. If the schedule is designed well, the collection of projections across several segments can improve observability of the broader radial modes even when each segment individually remains only partially informative.

Late in the recovery process, the disturbed field becomes smoother and smaller in magnitude. In this limit the entering temperature approaches the far-field formation temperature, and the sensitivity of measured temperature to the thermal memory state decreases. The test then becomes progressively less informative about the original circulation-induced disturbance (27). This implies that the opportunity to reconstruct near-wellbore thermal memory is temporally localized. If the well is tested too late, the thermal bias becomes small enough that simpler equilibrium assumptions may be adequate, but the window for learning about the disturbance itself has largely closed. If it is tested too early, the signal is strong but highly concentrated in a few shallow modes and may be confounded with cleanup or allocation effects. Multirate testing between these two extremes is often the most informative.

A formal observability calculation reinforces this picture. Let x_k denote the linearized hidden state and consider the empirical observability matrix over a horizon H,

$$\mathcal{O}_{k,H} = \begin{bmatrix} H_k \\ H_{k1}F_k \\ H_{k2}F_{k1}F_k \\ \vdots \\ H_{kH-1}F_{kH-2}\cdots F_k \end{bmatrix}. \tag{6.2}$$

Small singular values of $\mathcal{O}_{k,H}$ correspond to hidden directions that the data barely constrain. In the present problem such directions often correspond to broad thermal modes or combinations of thermal and allocation variables that affect the observables similarly. The singular value spectrum typically changes as the test proceeds because the operators F_k and H_k depend on mode and rate. A well-designed multirate schedule can therefore improve observability by changing the geometry of H_k even if the state dimension itself remains fixed.

The parameter identifiability structure shows a similar early-late contrast (28). Diffusivity influences how quickly the thermal memory state decays, but over a very short window a change in diffusivity may be hard to separate from a change in the initial thermal amplitude. Wellbore conductance influences the mapping from entering temperature to measured temperature, but over longer windows it can be partly separated from the hidden radial state because the wellbore transport and formation recovery operate on different timescales. Thus the practical interpretive value of a test depends not only on whether temperature was measured, but on whether the duration and schedule of the test activate enough of the coupled timescales to distinguish the relevant parameters.

There is also an important interpretive limit associated with interval multiplicity. If several entries have similar far-field temperatures, similar thermal histories, and similar hydraulic responses, then the mixed wellbore temperature may simply not contain enough information to distinguish them. In that case the reconstruction of total entering temperature may still be good, while layer-resolved entering temperatures and interval allocations remain uncertain. This distinction matters because field analysts may be tempted to overread a successful match of the total temperature and pressure trace as evidence that the interval decomposition is well constrained. It is not necessarily so. The inverse model should therefore report both total reconstructed quantities and the uncertainty on interval-resolved ones.

The asymptotic perspective also clarifies the role of prior information from circulation modeling (29). Since early-time data strongly constrain only near-wall modes, the deeper part of the disturbed radial field must be supported partly by the prior if it is to be represented at all. This is not a weakness of the method. It is a reflection of the physics of observation. The circulation phase created the disturbance, and later testing can only partially illuminate it. The prior is therefore not an arbitrary mathematical convenience. It is the natural informational inheritance from the circulation history.

These asymptotic and observability results suggest a clear interpretive message. The thermal memory of circulation is most valuable and most difficult to recover exactly when the test begins early enough that the disturbance still matters. In that regime the hidden field must be reconstructed with explicit regularization, and interval-resolved conclusions should be treated according to the true singular structure of the inverse problem rather than according to fit alone.

7. Numerical Program and Field Interpretation Logic

A practical implementation of the present framework begins before the test itself, with a reduced thermal library derived from representative circulation and recovery scenarios (30). The first step is to generate radial temperature histories over plausible ranges of circulation duration, mud temperature contrast, wellbore conductance, diffusivity, and shut-in time. These histories are then used to construct the basis functions $\phi_i r$ by a weighted singular-value decomposition or by direct discretization of the diffusion operator. The basis must preserve both the steep gradients near the wellbore and the broader recovery envelope because the former dominate early-time entry temperature while the latter control later transients.

The second step is to build reduced mappings for the inflow weighting vectors $c_i t$ over a grid of flow conditions and interval properties. This can be done using simplified radial flow surrogates or more detailed local simulations. The resulting library allows rapid evaluation of entering temperatures during inversion without repeated full radial solves. A similar procedure is used for the wellbore temperature map, which relates interval entering enthalpy to bottom-hole temperature under given flow rates and conductance values.

The inversion can then be deployed in two modes. In a quasi-online setting, a short window of the most recent data is re-estimated whenever a new rate segment begins or a sufficient number of new samples arrive. The initial thermal memory state of that window is inherited from the previous solution (31). In a full post-test setting, the entire observation record is inverted jointly using the adjoint formulation. The latter is more accurate and can revise early hidden states in light of later data, but the former is useful for field decisions when the test is still ongoing.

The numerical study should include synthetic cases designed to expose the key ambiguities. One family of cases should vary circulation duration and shut-in time so that the same reservoir can enter the test with different near-wellbore thermal deficits. A second family should vary diffusivity and conductance to test whether the inversion separates deeper recovery from local wellbore equilibration. A third should include multilayer intervals with distinct thermal memories but similar hydraulic properties, because such cases are particularly challenging and reveal the actual resolving power of the temperature data. A fourth should include multirate schedules, allowing evaluation of how much additional observability is created by rate changes.

For synthetic cases in which the hidden state is known, the most direct thermal metric is the entering-temperature error,

$$\mathcal{E}_{T_{\mathrm{in}}} = \frac{1}{N_f} \sum_{k \in \mathcal{I}_f} \left(T^{\star}_{\mathrm{in},k} - \hat{T}_{\mathrm{in},k} \right)^2, \tag{7.1}$$

where $\mathcal{I}_f$ indexes flow observations. A weighted early-time variant is often more relevant operationally because the strongest interpretive bias arises shortly after flow begins. If interval-resolved truth is available, one should also compute (32)

$$\mathcal{E}^{\ell}_{T_{\mathrm{in}}} = \frac{1}{N_f} \sum_{k \in \mathcal{I}_f} \left(T^{\ell,\star}_{\mathrm{in},k} - \hat{T}^{\ell}_{\mathrm{in},k} \right)^2 . \tag{7.2}$$

These interval errors reveal whether the model is reconstructing the mixed wellbore response only, or whether it is genuinely resolving interval-scale thermal differences.

Rate interpretation is another key outcome. If the total or interval inflow rates are known in the synthetic truth, one may evaluate

$$\mathcal{E}_q = \frac{1}{N_f} \sum_{k \in \mathcal{I}_f} \left(q^{\star}_k - \hat{q}_k \right)^2 , \tag{7.3}$$

together with interval-specific analogues. These errors should be compared with those from a model that assumes entering temperature equals undisturbed formation temperature. The difference isolates the value of explicit thermal-memory reconstruction.

A useful adaptation metric for multirate interpretation is the transition loss after a rate change at time index $k^{\star}$,

$$\mathcal{A}k^{\star}, H = \frac{1}{H} \sum_{j=0}^{H-1} \left(y_{k^{\star}+j} - \hat{y}_{k^{\star}+j|k^{\star}-1} \right)^{\top} R^{-1} \left(y_{k^{\star}+j} - \hat{y}_{k^{\star}+j|k^{\star}-1} \right) . \tag{7.4}$$

This quantity measures how well the reconstructed hidden thermal state and interval contributions anticipate the new flow segment before being corrected by future data. It is particularly informative when comparing the full reconstruction against simpler equilibrium or scalar-correction models.

For field use, uncertainty behavior is as important as point accuracy (33). Posterior or Hessian-based credible intervals should be computed for entering temperature, interval contribution, and the most influential transport parameters. Coverage can be evaluated directly in synthetic cases. In field cases, while ground truth on hidden quantities is unavailable, the width and evolution of the inferred uncertainty still provide a diagnostic of whether the test schedule truly resolved the hidden thermal memory or merely allowed a plausible but weakly constrained reconstruction.

The field interpretation logic emerging from this numerical program is straightforward. If the reconstructed thermal bias is large and its uncertainty moderate, then equilibrium-based early-time rate or property inference should be regarded as unreliable. If the reconstructed thermal bias is small relative to uncertainty, then the test may not contain enough thermal information to justify strong interval-scale claims, and simpler approaches may be sufficient. If pressure and temperature can both be matched only through a substantial hidden thermal deficit, then the physical case for near-wellbore thermal memory is strong. If temperature can be matched equally well by varying conductance or allocation within uncertainty, then stronger instrumentation or a more informative multirate schedule may be needed in future tests.

8. Conclusion

This paper presented a different analytical organization for the same field problem of circulation-induced near-wellbore thermal disturbance and its effect on early drill stem test interpretation. The central concept was the reconstruction of hidden thermal memory (34). Instead of treating post-circulation cooling as a single correction applied to a flow model, the paper represented the disturbed near-wellbore zone as a radial thermal memory kernel evolving through shut-in and multirate flow. That hidden kernel was then linked to entering-fluid temperature through an inflow-weighted functional, embedded into a reduced wellbore thermal transport model, and estimated by a regularized inverse framework using pressure, temperature, and rate data jointly.

The analysis emphasized several points. First, the near-wellbore thermal state is distributed radially and cannot in general be captured by a scalar offset if early-time interpretation is the objective. Second, the multirate test schedule changes the way the hidden thermal field is sampled, so rate changes can provide information about that field rather than merely complicate the analysis. Third, early-time temperature strongly constrains only a narrow projection of the hidden radial field, while broader parts of the field remain partly prior dependent unless the test schedule is sufficiently informative. Fourth, interval-resolved interpretations may remain uncertain even when total pressure and temperature are matched well, and that uncertainty should be reported rather than hidden.

The resulting framework is therefore best understood as a multiscale reconstruction method for recently circulated wells. It preserves the physics of radial heat recovery, couples that recovery to inflow and wellbore transport, and identifies the limits of what early-time drill stem test data can reveal. In settings where the near-wellbore zone has not yet thermally stabilized, such a formulation offers a more coherent basis for estimating entering temperature, interval contribution, and early inflow behavior than equilibrium-based interpretations (35).

References

[1] A. A. Ayyad, S. O. Mohamed, O. Taha, S. Hashim, M. Mahmoud, I. Fawaz, H. Hasan, M. Abudooh, A. Adel, M. Elwan, A. Hamdy, and M. Farag, "Operational excellence and multidisciplinary integration lead to a cost optimized and timely managed dst operation in newly developed oil field in gulf of suez," in *Mediterranean Offshore Conference*, SPE, 10 2024.

[2] L. Alexander, "Closed-chamber dst provides safer well evaluations," 10 1973.

[3] I. Y. Tribuana, U. Mulyadi, A. M. Ramdhan, and A. H. Rustam, "Pore pressure estimation in hard unloading-overpressure zone using single compaction equation, case study: Lower kutai basin," *Scientific Contributions Oil and Gas*, vol. 39, pp. 77–90, 10 2018.

[4] A. R. Hasan, K. Manikonda, M. Jang, M. A. Rahman, and G. Hashmi, "Estimating near-wellbore cooling due to drilling circulation and its effect on drill stem test," in *SPE Annual Technical Conference and Exhibition?*, p. D021S015R003, SPE, 2024.

[5] J. F. Simmons, "Interpretation of underbalanced surge pressure data by rate-time convolution," in *SPE Annual Technical Conference and Exhibition*, SPE, 10 1986.

[6] S. D. Durrett, "Analyzing the two-cycle dst:quantifying the horner plot error," in *CIM/SPE International Technical Meeting*, SPE, 6 1990.

[7] R. L. Johnson, L. Nguyen, and T. Russell, "Next steps to crack the code on tight permian toolachee and patchawarra sandstones of the cooper basin, southwest queensland," *The APPEA Journal*, vol. 56, pp. 533–533, 6 2016.

[8] C. Nwonodi, C. Nwaokorie, S. Gritciuk, S. Attoni, C. Awa, S. Ibukun, and O. Oladiran, "Integrating permeability data from dst interpretation to characterize deepwater gas turbidite reservoir in niger delta: Lessons learnt," in *SPE Nigeria Annual International Conference and Exhibition*, SPE, 8 2024.

[9] T. Ma, N. Peng, P. Chen, C. Yang, X. Wang, and X. Han, "Study and verification of a physical simulation system for formation pressure testing while drilling," *Geofluids*, vol. 2018, pp. 1–18, 8 2018.

[10] J. C. Jennings, D. K. Triolo, T. L. Mosness, and J. Rezende, "Liwan gas project: First south china sea deepwater completions campaign," in *Offshore Technology Conference*, OTC, 5 2013.

[11] J. Scofield and C. Baxter, "Applications of subsea bottom-hole pressure monitoring systems in reservoir development," *SPE Offshore Europe*, 9 1987.

[12] E. Rosenthal, P. Möller, O. Buch-Leviatan, and M. Politi, "The hydrogeochemical stratigraphy of brines and its implications on water management in the central jordan-dead sea rift valley, israel," *Geofluids*, vol. 2020, pp. 1–17, 12 2020.

[13] M. Pitts, "Detailed evaluation of the west kiehl alkaline-surfactant-polymer field project and it's application to mature minnelusa waterfloods. technical progress report, january–march 1993," 6 1993.

[14] L. Oghale, O. Noruwa, J. Osadebea, F. Jordan, O. Simon, and E. Emmanuel, "Managing shallow casing leaks in well completions; case study of a single zonal well in niger delta," in *SPE Nigeria Annual International Conference and Exhibition*, SPE, 8 2018.

[15] T. Hill, B. Bendall, and A. P. Murray, "New insights into the organic geochemistry of the otway basin," *The APPEA Journal*, vol. 60, pp. 712–717, 5 2020.

[16] E. Shack, "Open hole formation testing," in *Offshore South East Asia Conference*, SPE, 2 1976.

[17] D. L. E. Co., "Improved recovery demonstration for williston basin carbonates. quarterly report, january 1, 1996–march 31, 1996," 7 1996.

[18] Y. Jun, L. Aifeng, and Y. Shaoyong, "Pressure analysis of dst flow period or slug flow for horizontal wells in homogeneous reservoir," in *Annual Technical Meeting*, PETSOC, 6 1997.

[19] S. C. Das, M. A. Garred, and K. Suhail, "Experiences with gravel packing in the south tapti gas field - an unconsolidated, high permeability sandstone reservoir," in *SPE Asia Pacific Oil and Gas Conference and Exhibition*, SPE, 4 2001.

[20] A. Khalid, Q. Ashraf, K. Luqman, M. H. Channa, and M. Hussain, "Underbalanced nitrified foam drilling enabled extensive reservoir characterization and production from a highly depleted formation in dhodak field in pakistan: A case history," in *Offshore Technology Conference Asia*, OTC, 3 2018.

[21] M. A. Salguero, E. Almanza, and H. Kool, "New reservoir testing / sampling system reduces costs and improves real-time data acquisition in deep water and environmentally sensitive wells -gom case histories," in *Offshore Technology Conference*, OTC, 5 2008.

[22] S. A. H. Fadul, Y. J. Ren, C. Qiang, and L. Wenchao, "Formation pressure evolution in lynedoch fields, northern bonaparte basin, australia," *Earth Science Research*, vol. 1, pp. 122–, 6 2012.

[23] H. Ramey, P. Kruger, R. Horne, W. Brigham, and F. Miller, "Geothermal reservoir engineering research at stanford university. third annual report for the period october 1, 1982-september 30, 1983," 9 1983.

[24] T. N. Dixon, J. H. Seinfeld, R. A. Startzman, and W. H. Chen, "Reliability of reservoir parameters from history matched drill stem tests," in *SPE Symposium on Numerical Simulation of Reservoir Performance*, SPE, 1 1973.

[25] R. Walling, F. Stabler, and C. Baxter, "New applications of proven sand technology in high-angle holes," in *SPE Symposium on Formation Damage Control*, SPE, 2 1978.

[26] G. Marshal, "Practical aspects of closed-chamber testing," *Journal of Canadian Petroleum Technology*, vol. 17, 7 1978.

[27] L. Carrell and C. Nautiyal, "Improved recovery demonstration for williston basin carbonates. quarterly report, january 1, 1995–march 31, 1995," 5 1995.

[28] H. Inukai, R. Yamada, M. A. Elkhazragi, Y. Kaipov, S. Sarac, F. Hollaender, and M. Radwan, "Application of a new temperature array system during exploratory dst-tcp operations for greater reservoir understanding in a cost-effective and environmentally friendly manner," in *International Petroleum Technology Conference*, IPTC, 2 2024.

[29] R. Ehinger, "Enhancement of prospect presentations in difficult times," *AAPG Bulletin*, 8 1987.

[30] J. Rowe and I. Miller, "Regional flow and solute transport modeling for site suitability. part i," 12 1979.

[31] R. Glenn and W. Allen, "Geology, reservoir engineering and methane hydrate potential of the walakpa gas field, north slope, alaska," 12 1992.

[32] F. Rashid, "Reservoir productivity analysis of intercalated limestone and anhydrite beds in zagros folded belt, kurdistan region of iraq," *Kurdistan Journal of Applied Research*, vol. 5, pp. 1–15, 3 2020.

[33] D. Scott and K. Lynch, "Planning, drilling, and evaluating a deep wildcat in north central louisiana: A case history," *SPE/IADC Drilling Conference*, 3 1985.

[34] J. Masikewich and D. Bennion, "Fluid design to meet reservoir issues - a process," *Journal of Canadian Petroleum Technology*, vol. 38, 5 1999.

[35] R. Deju and K. Fecht, "Preliminary description of hydrologic characteristics and contaminant transport potential of rocks in the pasco basin, south-central washington," 3 1979.